# A Rotation-Resilient Wireless Charging System for Lightweight Autonomous Underwater Vehicles

Tianze Kan, *Student Member, IEEE*, Yiming Zhang, *Member, IEEE*, Zhengchao Yan, *Student Member, IEEE*, Patrick P. Mercier, *Senior Member, IEEE*, and Chunting Chris Mi, *Fellow, IEEE*

***Abstract*—This paper presents a rotation-resilient wireless charging system with a reversely wound receiver that supports efficient charging for lightweight autonomous underwater vehicles. By employing a two-part reversely wound receiver coil structure, the total mutual inductance of the proposed coil structure remains relatively constant when rotational misalignment between the transmitter and receiver coils occurs, thereby ensuring wireless charging power is nearly continuous during rotational misalignment. Finite element analysis was performed with ANSYS Maxwell to verify the proposed coil structure. Double-sided LCC compensation topology was applied and circuit analysis was conducted via a mesh current method. A prototype of the rotation-resilient wireless charging system with the proposed coil structure was built and tested. Experimental results are well-matched to simulations, demonstrating that the system can deliver 745 Watts at a dc-dc efficiency of 86.19% when the system is fully aligned, and efficient under worst-case rotational misalignment.**

***Index Terms*—Wireless Power Transfer, Magnetic Coupling, Autonomous Underwater Vehicles, Rotational Misalignment.**

## I. Introduction

MAGNETIC resonance-based wireless power transfer has been widely applied in charging electric vehicles [1]–[3], consumer electronics [4]–[5], and biomedical implants [6]–[8]. Wireless charging of autonomous underwater vehicles (AUVs) is also an important application [9]–[17]. Since the mission tournament time of an AUV can be significantly increased via efficient and high-power wireless charging, and since the surrounding seawater environment makes for unique challenges relative to the other well-studied areas, this paper focuses on wireless charging of AUVs.

Research in this field started with Freezor *et al*. [9] and has been expanded into multiple directions since. For example, some researchers targeted improving the transferred power level with high efficiency: Kojiya *et al*. developed a cone-type coil structure and wirelessly delivered 500 Watts at a coil-to-coil efficiency of 93.1% [11]; Li *et al*. performed reluctance modeling and conducted experiments on a wireless charger with a planar coil structure, achieving 400 Watts of power transfer at a DC-DC efficiency of 90% [12]; Cheng *et al*. proposed a semi-closed magnetic core structure, analyzed the power loss, and built an underwater wireless charging system to transfer 10 kW at a DC-DC efficiency of 91% [13]. However, such work did not carefully consider the compatibility of the AUV's hull – the hull resistance in such cases may increase after installation, and, as a result, the AUV's speed might be reduced. As a result, other researchers have aimed at designing hull-compatible coil structure and addressing the AUV's hull resistance increase after coil structure's installation: Shi *et al*. presented a coaxial coil structure which could be installed around the AUV's hull with few adverse effects and established a prototype to transfer 45 Watts at 84% efficiency [14]; Lin *et al*. further studied the coaxial structure, performed the loss analysis, and enhanced the output power to 300 Watts with an efficiency of 77% [15]. In general, a coaxial coil arrangement showed good compatibility with the AUV's hull and efficiency was acceptable; however, the generated magnetic field was divergent within the hull, and thus might adversely affect electronic instrumentation within the AUV. Thus, Kan *et al*. proposed a wireless charging system with a hull-compatible three-phase coil structure, studied the magnetic field distributions, and demonstrated that the concentrated magnetic field had less impact on the instrumentation within the AUV. Moreover, a prototype was built and tested, demonstrating 1.0 kW of power transfer at a DC-DC efficiency of 92.41%. However, the system was very sensitive to rotational misalignment and thus would require an advanced mechanical positioning system, which would increase overall deployment cost [16].

The undersea environment is not as stable as the ambient air condition and rotational misalignments always occur when an AUV is being wirelessly charged in the docking station. In order to solve this problem with a relatively low cost, in this paper we propose a hull-compatible coil structure with a reversely wound receiver to improve the system performance during rotational misalignment between the transmitter and receiver coils. Finite

Manuscript received February 5, 2018; revised April 19, 2018; accepted May 7, 2018. Date of publication May 15, 2018; date of current version August 13, 2018. This work was supported by DOE GATE GRANT. The review of this paper was coordinated by Dr. B. Akin. *(Corresponding author: Chunting Chris Mi.)*

T. Kan is with the Department of Electrical and Computer Engineering, San Diego State University, San Diego, CA 92182 USA, and also with the Department of Electrical and Computer Engineering, University of California San Diego, La Jolla, CA 92093 USA (e-mail: tikan@eng.ucsd.edu).

Y. Zhang and C. C. Mi are with the Department of Electrical and Computer Engineering, San Diego State University, San Diego, CA 92182 USA (e-mail: zhangym07@gmail.com; mi@ieee.org).

P. P. Mercier is with the Department of Electrical and Computer Engineering, University of California San Diego, La Jolla, CA 92093 USA (e-mail: pmercier@ucsd.edu).

Z. Yan is with the Department of Electrical and Computer Engineering, San Diego State University, San Diego, CA 92182 USA, and also with the Northwestern Polytechnical University, Xi'an 710000, China (e-mail: yanzc1991@gmail.com).

Color versions of one or more of the figures in this paper are available online at http://ieeexplore.ieee.org.

Digital Object Identifier 10.1109/TVT.2018.2836988

element analysis is applied to verify the mutual inductance of the proposed coil structure is minimally affected during rotational misalignment. A prototype of the wireless charging system with the proposed coil structure is built and the experiment is conducted. It is demonstrated by the simulation and experimental results that the wireless charging system with the proposed coil structure has superior performance on rotational misalignment over the previous three-phase coil structure in [16]. This paper is organized as: Section I gives the introduction, Section II provides the coil design, Section III performs the circuit analysis, Section IV presents the experiment and Section V draws the conclusions.

## II. Coil Design

### A. Ideal Coil Design

The winding configuration and geometry of coils in a wireless power transfer system are of great importance, as they determine the power transfer performance and the magnetic field pattern. In order to improve the system performance on rotational misalignment, a rotation-resilient ideal coil structure with a reversely wound receiver is proposed as shown in Fig. 1(a). It consists of three identical transmitters and one receiver that is composed of two cores. The three transmitters are excited by three alternating currents with the same magnitude and frequency, but 120° out of phase. The receiver is divided into two parts connected in series: receiver part I and receiver part II. They have the same ferrite core and the same number of turns, but their winding directions are reversed from each other. The magnetic fluxes generated by the three transmitters couple with the receiver separately and return to the respective transmitters. As a result, there are three mutual inductances between each transmitter and the receiver. Since receiver parts I and II are reversely wound, the sum of the three mutual inductances is not zero. Furthermore, as will be shown shortly, it remains relatively constant when rotational misalignment occurs. Fig. 1(b) gives the overview of the simulation model, in which the three transmitters with water-resistant design are placed in seawater and the receiver is fixed within the AUV's hull. The hull is made of fiberglass and has an outer diameter of 200 mm.

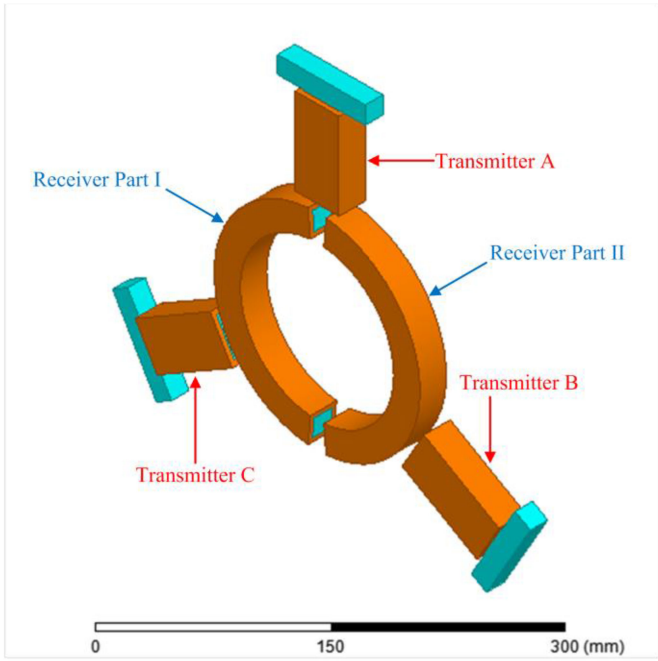


(a)

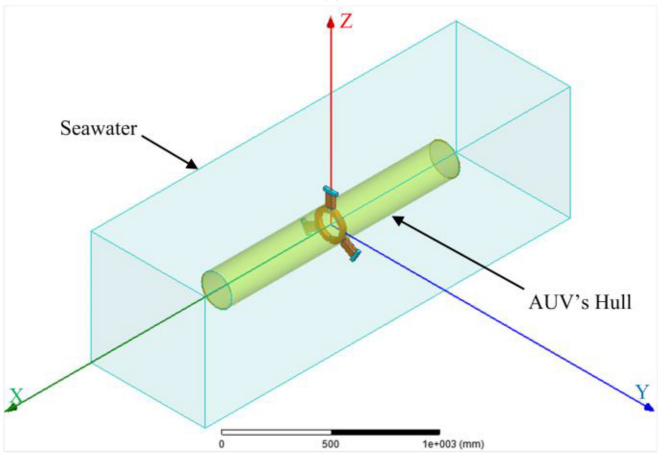


(b)

Fig. 1. Overview. (a) Of proposed ideal coil structure. (b) Of simulation model.

Simulation studies on rotational misalignment are conducted to verify the proposed ideal coil structure. Concurrently, a simulation model of the previous three-phase coil structure with three receivers in [16] is built and the system performances on the rotational misalignment are compared. In order to make a fair comparison, the seawater, the hull, and the transmitters are the same for both models. The magnitudes of the transmitter currents and the output powers are also the same. The only difference is in the receiver: the proposed ideal coil structure employs one receiver with two reversely wound parts, while the previous one uses three separate receivers. However, the number of turns of the receiver coil in the proposed ideal coil structure is the same as the total number of turns of the three receivers in the previous coil structure.

Power relies on the mutual inductance between the transmitter and the receiver to be transferred, thus, the mutual inductances are compared. For each receiver, there are three mutual inductances and the sum of the three mutual inductance vectors determines the power transferability. The equivalent mutual inductance $M_{\mathrm{eq}}$ is defined as the magnitude of the sum of the three mutual inductance vectors for each receiver and expressed as Eq. (1), shown at the bottom of this page, where $M_{\mathrm{AR}}$ stands

$$M_{\mathrm{eq}} = \left| M_{\mathrm{AR}} \cdot e^{j\cdot 0} + M_{\mathrm{BR}} \cdot e^{-j\cdot \frac{2\cdot\pi}{3}} + M_{\mathrm{CR}} \cdot e^{-j\cdot \frac{4\cdot\pi}{3}} \right| = \sqrt{M_{\mathrm{AR}}^2 + M_{\mathrm{BR}}^2 + M_{\mathrm{CR}}^2 - M_{\mathrm{AR}} M_{\mathrm{BR}} - M_{\mathrm{BR}} M_{\mathrm{CR}} - M_{\mathrm{CR}} M_{\mathrm{AR}}} \tag{1}$$

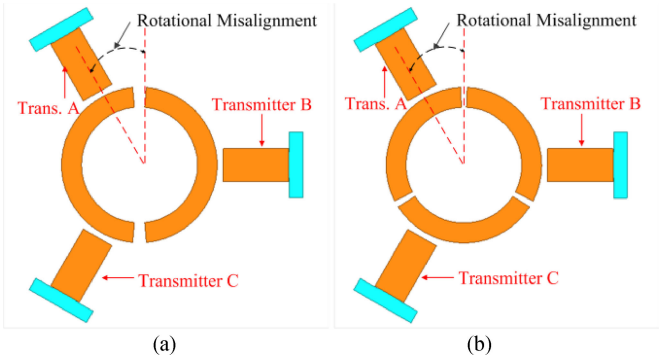


Fig. 2. Rotational misalignments. (a) In proposed ideal coil structure. (b) In previous coil structure.

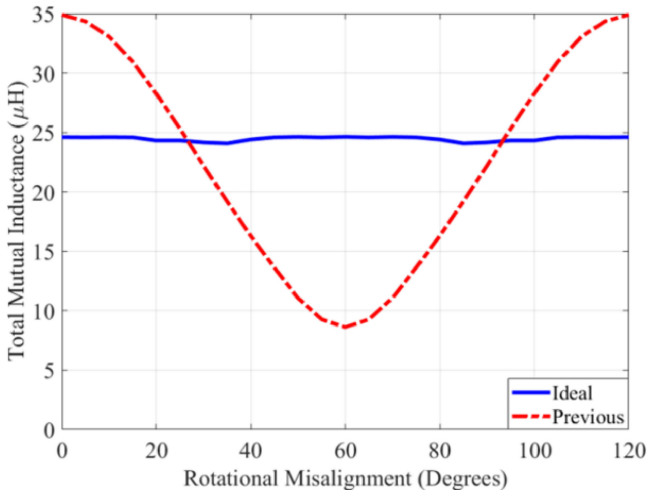


Fig. 3. Total mutual inductances over rotational misalignment for proposed ideal coil structure and the previous coil structure from [16].

for the mutual inductance value between Transmitter A and the receiver, and likewise, $M_{BR}$ and $M_{CR}$. For the proposed coil structure, the total mutual inductance, $M_{tot}$, is the equivalent mutual inductance, $M_{eq}$. For the previous coil structure with three receivers, the total mutual inductance, $M_{tot}$, is the sum of the three equivalent mutual inductances.

Rotational misalignment is depicted in Fig. 2, in which the transmitters rotate counterclockwise while the respective positions of the three transmitters are fixed. For the proposed ideal coil structure, when the system is fully aligned, $M_{AR}$ reaches its maximum while $M_{BR}$ and $M_{CR}$ are multiple times smaller. It is because magnetic coupling occurs near the coil structure and near Transmitter A, the part of receiver is reversely wound. Therefore, the coupling is strong and the mutual inductance is large. While the parts of receiver at Transmitters B and C are wound in the same direction, the couplings are weaker and the mutual inductances are smaller. Power thus mainly relies on $M_{AR}$ to be transferred. As the rotational misalignment increases from 0° to 30°, $M_{AR}$ and $M_{BR}$ decrease while $M_{CR}$ increases. Here, power mostly relies on $M_{AR}$ and $M_{CR}$ to be transferred. As the rotational misalignment continues increasing to 60°, $M_{CR}$ goes up to the maximum and power primarily relies on $M_{CR}$ to be transferred, which is the same with the fully aligned case. For the previous coil structure, the total mutual inductance decreases from the maximum to the minimum when the rotational misalignment increases from 0° to 60° and goes up to the maximum as the rotational misalignment increases to 120°.

Simulations with rotational misalignments are conducted and the total inductances are compared in Fig. 3. In the fully aligned condition, the total mutual inductance of the proposed ideal coil structure is smaller than that of the previous coil structure. It is because power mainly relies on $M_{AR}$ to be transferred while $M_{BR}$ and $M_{CR}$ are multiple times smaller. As the rotational misalignment increases from 0° to 120°, the total mutual inductance of the proposed coil structure is almost constant while that of the previous coil structure decreases from its maximum to 25% of the maximum value, and increases back to its maximum. If the rated powers of the two coil structures are both 1.0 kW, the output power of the proposed ideal coil structure remains 1.0 kW while that of the previous coil structure changes from 1.0 kW to 250 Watts as the rotational misalignment varies from 0° to 120°. In addition, simulation results demonstrate the mutual inductances between each two phases of transmitters are 0.84 $\mu$H, which is much smaller compared to the total mutual inductance of 25 $\mu$H. Therefore, we neglect the mutual inductances between each two phases of the transmitters in the following analysis.

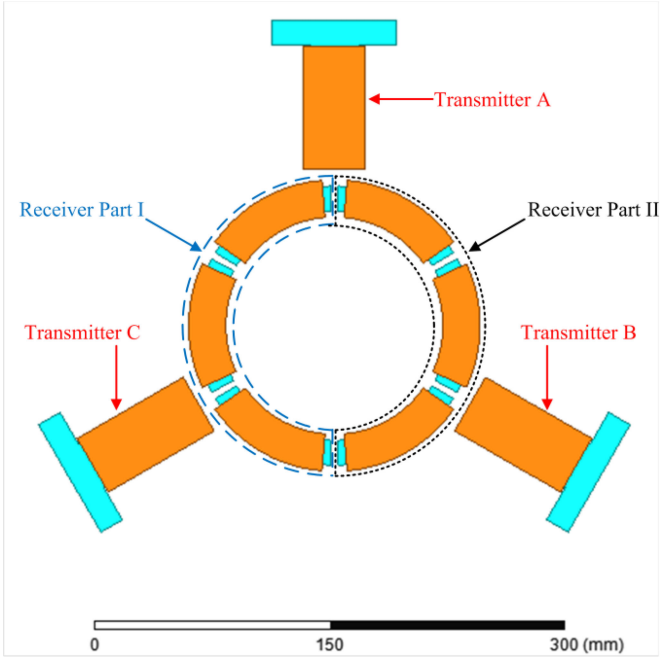


Fig. 4. Proposed segmented coil design.

### B. Segmented Coil Design

In practice, it is very difficult to find two large arc-shaped ferrite cores or their substitutions for experiments. Instead, the smaller pieces of arc-shaped ferrite cores are employed in this part to minimize the difference between simulation and experiment. As shown in Fig. 4, each part of the receiver has three segmented coils. Within the same receiver part (i.e., part I or II), the three segmented coils are wound in the same direction

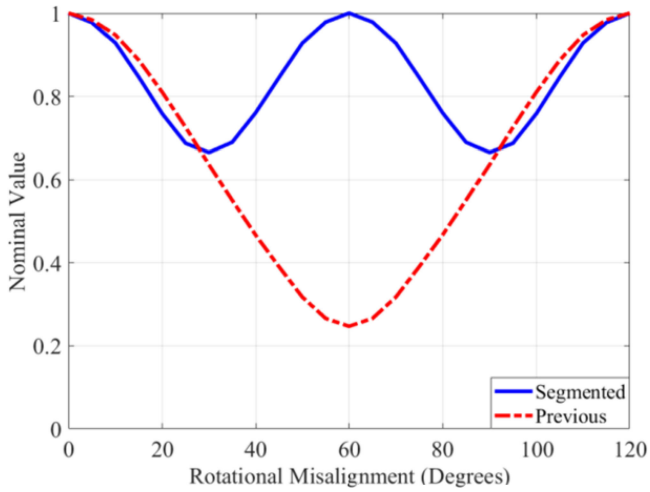


Fig. 5. A comparison between the nominal value of the total mutual inductances in proposed segmented coil design and that in previous coil design over rotational misalignment.

and connected in series. Between different parts, the winding directions are reversed. The total number of turns of the receiver in the segmented coil design is the same as that in the ideal coil design. In addition, four or more segmented coils will work. We select six segmented coils since it is convenient for us to verify the proposed segmented coil structure in experiment using the ferrite bars available in lab.

Simulations are performed on rotational misalignment and the total mutual inductance in the segmented coil design is smaller than that of the ideal coil structure due to the segmented ferrite cores with air gaps between them. As a result, the receiver's self-inductance decreases and the coupling coefficients go down. However, the segmented coil structure still has superior performance over rotational misalignment since the largest variation is only 25%. Fig. 5 compares the nominal value of the total mutual inductance in the proposed segmented coil structure with that in the previous coil structure over rotational misalignment. If both two coil structures are nominally designed to transfer 1.0 kW, the output power of the proposed segmented coil structures ranges from 750 Watts to 1.0 kW when the rotational misalignment occurs – i.e., an output power variation of only 250 Watts. This compares favorably to the previous segmented design proposed in [16], whose output power can go as low as 250 Watts, for a total power variation of 750 Watts.

### C. Magnetic Field Distribution

The magnetic field distributions of the proposed coil structure in the fully aligned and the worst rotational misaligned conditions are plotted in Fig. 6. The scales of the magnetic flux densities are the same with those in [16]: $2.45 \times 10^{-3}$ T at the maximum and $1 \times 10^{-4}$ T at the minimum. The magnetic fields of the proposed coil structure are more divergent than those of the previous coil structure in [16], but still more convergent than the traditional coaxial coil structure. Therefore, the magnetic field distribution in the proposed coil structure is acceptable.

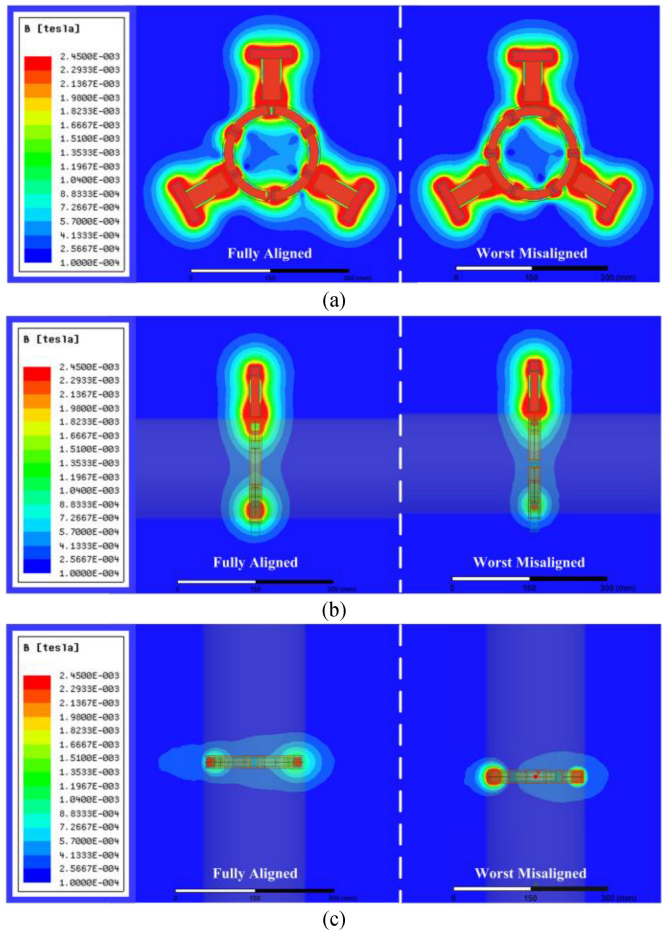


Fig. 6. Magnetic field distributions. (a) In YZ-plane. (b) In ZX-plane. (c) XY-plane at the fully aligned and worst misaligned conditions.

Furthermore, a simulation model in ambient air condition, in which the seawater and the AUV's hull are omitted, is built and simulation studies on coil parameters and magnetic field distributions are conducted. The simulation results in ambient air condition and seawater condition are almost the same. It is because the relative permeability of seawater is very close to 1 and the seawater can be considered as air at the frequency of interest. The experimental results in [16] further demonstrate that there is almost no difference between seawater and ambient air conditions. Therefore, the following analysis and experiment will be conducted in the ambient air condition.

## III. Circuit Analysis

Circuit analysis based on first harmonic approximation is performed from a DC power supply all the way to DC batteries on the AUV. Three full-bridge inverters are employed to generate three alternating voltages $u_{\mathrm{A}}$, $u_{\mathrm{B}}$, and $u_{\mathrm{C}}$, with the same magnitude and frequency, but 120° out of phase. A full-bridge rectifier is used to convert from AC to DC. The DC batteries are considered as a load resistor $R_{\mathrm{L}}$ in the analysis since the voltage of the batteries is constant when they are charged at the desired power. Fig. 7 shows the circuit diagram of the wireless charging system with the proposed coil structure and the

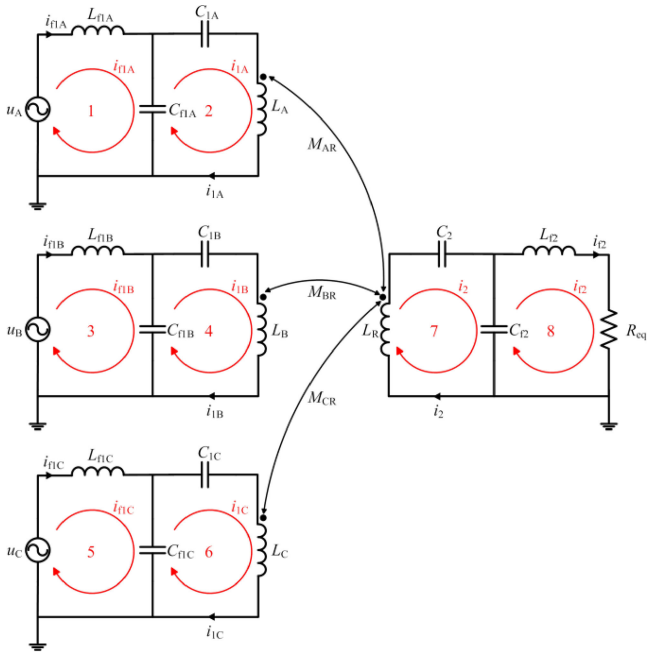


Fig. 7. Circuit diagram.

equivalent series resistances of the components are ignored. On the transmitter side, LCC compensation is selected to drive the transmitters, where the auxiliary coil resonates with the respective auxiliary capacitor, creating three currents with the same magnitude and frequency though 120° out of phase. When the rotational misalignment occurs, even though the three mutual inductances change and the reflected impedances from the receiver vary, the three currents remain the same. On the receiver's side, LCC compensation is also chosen to achieve constant current charging, which is desired for charging batteries [18], [19]. The resistor $R_{\mathrm{eq}}$ is the equivalent resistor of $R_{\mathrm{L}}$.

In Phase A, the auxiliary coil $L_{\mathrm{f1A}}$ is resonant with the auxiliary capacitor $C_{\mathrm{f1A}}$, and the transmitter's self-inductance $L_{\mathrm{A}}$ is combined with the primary main capacitor $C_{\mathrm{1A}}$ to resonate with $C_{\mathrm{f1A}}$, likewise for phase B and C. On receiver's side, the receiver's self-inductance $L_{\mathrm{R}}$ is cooperated with the secondary main capacitor $C_2$ to resonate with the secondary auxiliary capacitor $C_{\mathrm{f2}}$, and the secondary auxiliary coil $L_{\mathrm{f2}}$ is resonant with $C_{\mathrm{f2}}$. The resonant conditions can be expressed as

$$\begin{cases} j\omega L_{\mathrm{f1A}} + \dfrac{1}{j\omega C_{\mathrm{f1A}}} = 0, j\omega L_A + \dfrac{1}{j\omega C_{\mathrm{1A}}} + \dfrac{1}{j\omega C_{\mathrm{f1A}}} = 0 \\ j\omega L_R + \dfrac{1}{j\omega C_2} + \dfrac{1}{j\omega C_{\mathrm{f2}}} = 0, j\omega L_{\mathrm{f2}} + \dfrac{1}{j\omega C_{\mathrm{f2}}} = 0 \end{cases} \tag{2}$$

where $\omega$ is the angular frequency. As shown in Fig. 7, the circuit is divided into eight meshes and mesh current method is applied to the circuit. In the resonant condition, the matrix is derived as.

Three alternating voltages $u_{\mathrm{A}}$, $u_{\mathrm{B}}$, and $u_{\mathrm{C}}$ have the same magnitude of $U$. Moreover, in order to simplify the calculation, the primary auxiliary coils $L_{\mathrm{f1A}}$, $L_{\mathrm{f1B}}$, and $L_{\mathrm{f1C}}$ are assumed to be exactly the same and equal to $L_{\mathrm{f1}}$. Similarly, the primary auxiliary capacitors have the same value of $C_1$. By solving (3), shown at the bottom of this page, the currents are obtained as

$$\begin{bmatrix} i_{\mathrm{f1A}} \\ i_{\mathrm{1A}} \\ i_{\mathrm{f1B}} \\ i_{\mathrm{1B}} \\ i_{\mathrm{f1C}} \\ i_{\mathrm{1C}} \\ i_2 \\ i_{\mathrm{f2}} \end{bmatrix} = \begin{bmatrix} \frac{R_{\mathrm{eq}} M_{\mathrm{AR}} U \cdot \left[(2M_{\mathrm{AR}} - M_{\mathrm{BR}} - M_{\mathrm{CR}}) + j\cdot\sqrt{3}(M_{\mathrm{BR}} - M_{\mathrm{CR}})\right]}{2\omega^2 L_{\mathrm{f1}}^2 L_{\mathrm{f2}}^2} \\ -j\frac{U}{\omega L_{\mathrm{f1}}} \\ \frac{R_{\mathrm{eq}} M_{\mathrm{BR}} U \cdot [(2M_{\mathrm{AR}} - M_{\mathrm{BR}} - M_{\mathrm{CR}}) + j\cdot\sqrt{3}(M_{\mathrm{BR}} - M_{\mathrm{CR}})]}{2\omega^2 L_{\mathrm{f1}}^2 L_{\mathrm{f2}}^2} \\ \frac{(1+j\cdot\sqrt{3})\cdot U}{2\omega L_{\mathrm{f1}}} \\ \frac{R_{\mathrm{eq}} M_{\mathrm{CR}} U \cdot [(2M_{\mathrm{AR}} - M_{\mathrm{BR}} - M_{\mathrm{CR}}) + j\cdot\sqrt{3}(M_{\mathrm{BR}} - M_{\mathrm{CR}})]}{2\omega^2 L_{\mathrm{f1}}^2 L_{\mathrm{f2}}^2} \\ \frac{(\sqrt{3}+j\cdot 1)\cdot U}{2\omega L_{\mathrm{f1}}} \\ \frac{R_{\mathrm{eq}} U \cdot [(2M_{\mathrm{AR}} - M_{\mathrm{BR}} - M_{\mathrm{CR}}) + j\cdot\sqrt{3}(M_{\mathrm{BR}} - M_{\mathrm{CR}})]}{2\omega^2 L_{\mathrm{f1}}^2 L_{\mathrm{f2}}^2} \\ \frac{U \cdot [\sqrt{3}(M_{\mathrm{BR}} - M_{\mathrm{CR}}) - j\cdot(2M_{\mathrm{AR}} - M_{\mathrm{BR}} - M_{\mathrm{CR}})]}{2\omega L_{\mathrm{f1}} L_{\mathrm{f2}}} \end{bmatrix} \tag{4}$$

Therefore, the output power can be calculated as Eq. (5), shown at the bottom of this page.

If the power loss from the inverter and the rectifier is ignored and only the first harmonic is considered, according to [20], the output power from DC power supply to DC batteries is given in Eq. (6), shown at the bottom of the next page.

$$\begin{bmatrix} u_A \\ 0 \\ u_B \\ 0 \\ u_C \\ 0 \\ 0 \\ 0 \end{bmatrix} = \begin{bmatrix} 0 & -\frac{1}{j\omega C_{\mathrm{f1A}}} & 0 & 0 & 0 & 0 & 0 & 0 \\ -\frac{1}{j\omega C_{\mathrm{f1A}}} & 0 & 0 & 0 & 0 & 0 & -j\omega M_{\mathrm{AR}} & 0 \\ 0 & 0 & 0 & -\frac{1}{j\omega C_{\mathrm{f1B}}} & 0 & 0 & 0 & 0 \\ 0 & 0 & -\frac{1}{j\omega C_{\mathrm{f1B}}} & 0 & 0 & 0 & -j\omega M_{\mathrm{BR}} & 0 \\ 0 & 0 & 0 & 0 & 0 & -\frac{1}{j\omega C_{\mathrm{f1C}}} & 0 & 0 \\ 0 & 0 & 0 & 0 & -\frac{1}{j\omega C_{\mathrm{f1C}}} & 0 & -j\omega M_{\mathrm{CR}} & 0 \\ 0 & -j\omega M_{\mathrm{AR}} & 0 & -j\omega M_{\mathrm{BR}} & 0 & -j\omega M_{\mathrm{CR}} & 0 & -\frac{1}{j\omega C_2} \\ 0 & 0 & 0 & 0 & 0 & 0 & -\frac{1}{j\omega C_2} & R_{\mathrm{eq}} \end{bmatrix} \cdot \begin{bmatrix} i_{\mathrm{f1A}} \\ i_{\mathrm{1A}} \\ i_{\mathrm{f1B}} \\ i_{\mathrm{1B}} \\ i_{\mathrm{f1C}} \\ i_{\mathrm{1C}} \\ i_2 \\ i_{\mathrm{f2}} \end{bmatrix} \tag{3}$$

$$P_{\mathrm{o}} = |i_{\mathrm{f2}}|^2 \cdot R_{\mathrm{eq}} = \frac{R_{\mathrm{eq}} U^2 \cdot \left(M_{\mathrm{AR}}^2 + M_{\mathrm{BR}}^2 + M_{\mathrm{CR}}^2 - M_{\mathrm{AR}} M_{\mathrm{BR}} - M_{\mathrm{BR}} M_{\mathrm{CR}} - M_{\mathrm{CR}} M_{\mathrm{AR}}\right)}{\omega^2 L_{\mathrm{f1}}^2 L_{\mathrm{f2}}^2} \tag{5}$$

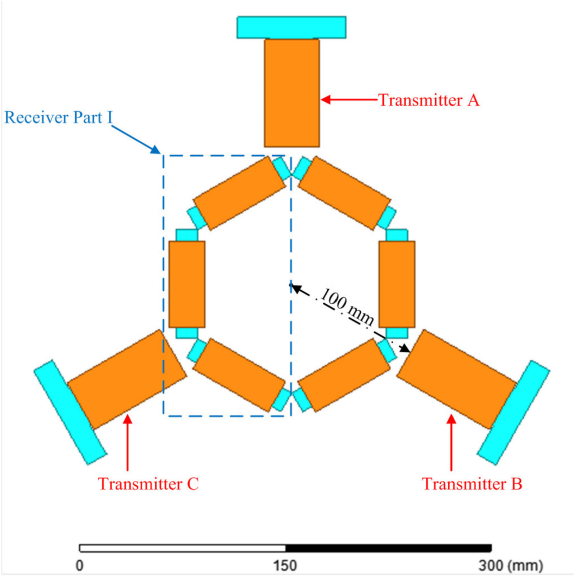


Fig. 8. Simulation model of the coil prototype.

As can been seen from (6), the results is aligned with (1). During rotational misalignment, the total mutual inductance remains constant and the output power is continuous.

## IV. Experiment

Experiments are conducted to verify the proposed coil structure. Due to the difficulty of getting arc-shaped ferrite magnets at the frequency of interest, ferrite bars are employed for receiver's core in the coil prototype. The simulation model of the coil prototype is shown in Fig. 8 and the simulations on rotational misalignment are performed in ambient air condition. Since 60° is the minimum period, the rotational misalignment changes from 0° to 60° in both simulation and experiment. A coil prototype is built based on the simulation model and the mutual inductances between the three transmitters and the receiver are measured during rotational misalignment. The total mutual inductance is calculated and compared with that in the simulation. The results are summarized in Fig. 9, which shows that measurements are well-matched to the simulations. As the rotational misalignment increases from 0° to 60°, the total mutual inductance decreases from its maximum value 10 $\mu$H to its minimum value 5 $\mu$H, and then increases back to 10 $\mu$H. In the prototype, the largest variation is approximately 50% and the variation can be minimized by using customized large or small segmented arc-shaped ferrite magnets in future work. The circuit parameters are designed based on (2) and (6) in Section III and measured by an LCR meter. The designed and measured results in the fully aligned condition are listed in Table I. The differences between the designed and measured values are very small.

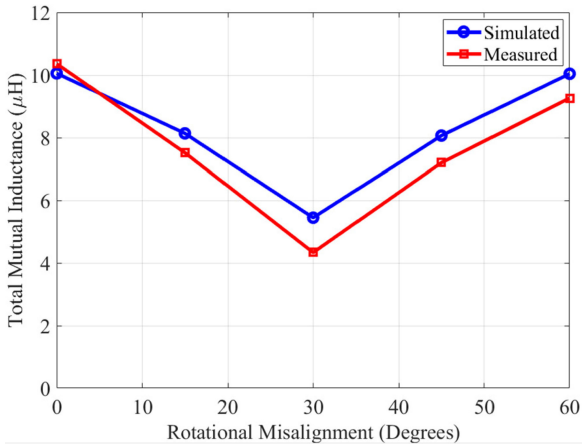


Fig. 9. Simulated and measured results of the total mutual inductances.

TABLE I
Circuit Parameters When Fully Aligned

| Coils (μH) | | | Capacitors (nF) | | | Mutual Ind. (μH) | | |
|---|---|---|---|---|---|---|---|---|
| Para. | Des. | Mea. | Para. | Des. | Mea. | Para. | Des. | Mea. |
| $L_{f1A}$ | 6.60 | 6.55 | $C_{f1A}$ | 16.25 | 16.34 | $M_{AR}$ | 8.23 | 8.12 |
| $L_{f1B}$ | 6.60 | 6.56 | $C_{f1B}$ | 16.25 | 16.38 | $M_{BR}$ | -1.83 | -2.47 |
| $L_{f1C}$ | 6.60 | 6.54 | $C_{f1C}$ | 16.25 | 16.36 | $M_{CR}$ | -1.82 | -2.00 |
| $L_{f2}$ | 5.80 | 5.81 | $C_{f2}$ | 18.49 | 18.59 | $M_{tot}$ | 10.05 | 10.36 |
| $L_A$ | 56.00 | 57.07 | $C_{1A}$ | 2.17 | 2.11 | | | |
| $L_B$ | 56.00 | 58.14 | $C_{1B}$ | 2.17 | 2.08 | | | |
| $L_C$ | 56.00 | 56.66 | $C_{1C}$ | 2.17 | 2.14 | | | |
| $L_R$ | 45.00 | 45.14 | $C_2$ | 2.74 | 2.73 | | | |

According to the circuit analysis in Section III, a three-phase wireless charging system using double-sided LCC compensation topology is built as shown in Fig. 10. Five rotational misalignments are selected: 0°, 15°, 30°, 45°, and 60°. Both the input DC voltage and the DC voltage of the electronic load are fixed at 110 V. The TI microcontroller TMS320F28335 is employed to generate 12 PWMs to drive the 12 MOSFETs in the three full-bridge inverters to achieve three square voltage waves with the same magnitude and frequency but 120 degrees out of phase. The switching frequency is 472 kHz, which makes the system compact and ensures enough power to be transferred. In order to alleviate the higher switching loss, copper loss, and core loss resulting from the high switching frequency, SiC devices are chosen to achieve soft switching, 3000-strand AWG-46 Litz wires are selected to minimize the skin effects, and 3C95 ferrite bars from Ferroxcube are employed due to its relatively low power loss at 500 kHz. The waveforms at 0° and 30° are shown in Fig. 11 and the system performance on the output power and the DC-DC efficiency over different rotational

$$P_o = \frac{8U_{in}U_o}{\pi^2\omega L_{f1}L_{f2}} \cdot \sqrt{M_{AR}^2 + M_{BR}^2 + M_{CR}^2 - M_{AR}M_{BR} - M_{BR}M_{CR} - M_{CR}M_{AR}} \quad (6)$$

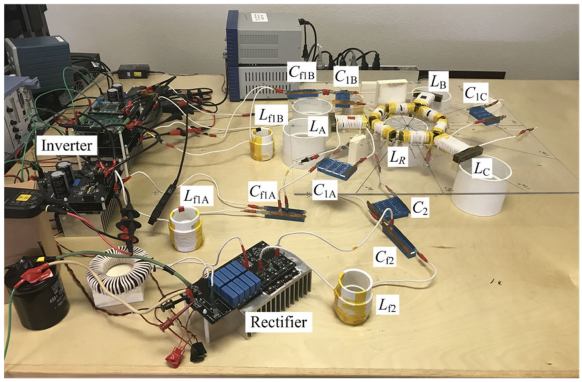


Fig. 10. Experiment setup of a wireless charging system with proposed coil structure.

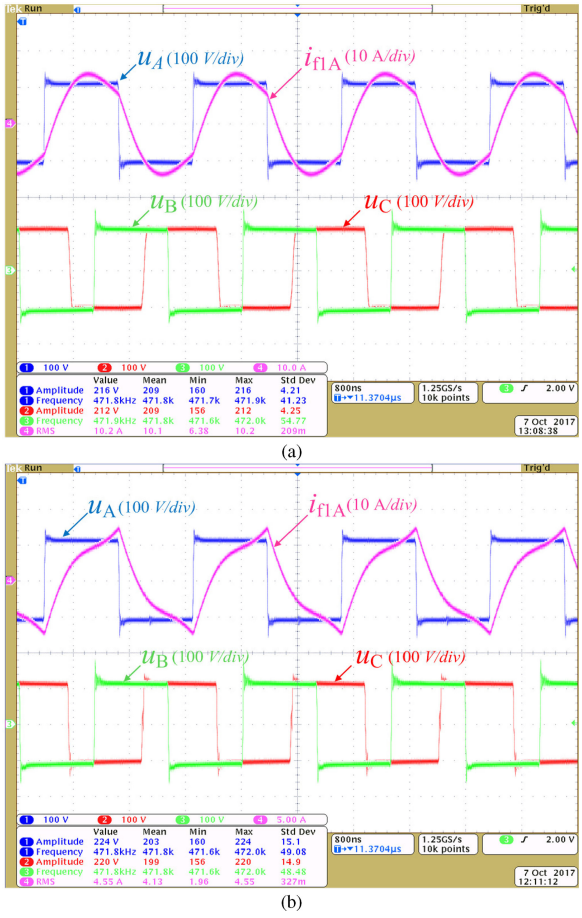


Fig. 11. Waveforms. (a) When system is fully aligned. (b) When rotational misalignment is 30°.

misalignments are plotted in Fig. 12. When the system is fully aligned, it delivers 745 Watts at a DC-DC efficiency of 86.19%. As rotational misalignment increases from 0° to 30°, the output power drops to 321 Watts since the total mutual inductance goes down to 4.33 $\mu$H. The efficiency decreases to 76.24%. This decrease occurs because the total mutual inductance decreases and more harmonics appear in the system, which can be seen from Fig. 11(b). The experimental result in the worst rotational misalignment is still good by comparing to the previous coil

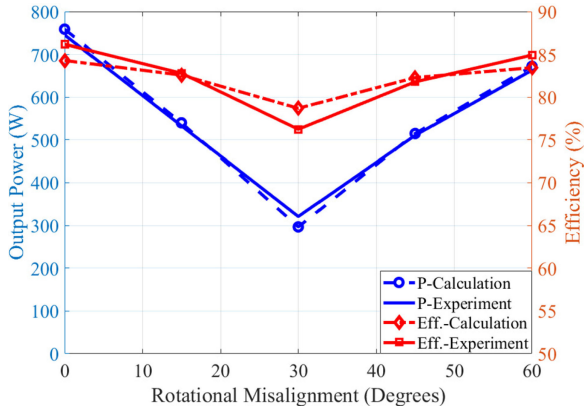


Fig. 12. Calculation and experimental results on output power and DC-DC efficiency over rotational misalignment.

structure in [16]. If the previous coil structure is designed to transfer 745 Watts when it is fully aligned, it will only deliver 187 Watts at most based on the simulation results in Section II. As the rotational misalignment continues increasing to 60°, both the output power and efficiency go up. As can be seen from the experimental results, the wireless charging system with the proposed coil structure is more immune to rotational misalignment than the design in [16]. Moreover, if arc-shaped ferrite magnets are customized in the future, system performance could be further improved.

In addition, in order to further verify the circuit analysis in Section III, the power loss of the system is analyzed. The power loss originates from power converters, coils, and capacitors. In the power converters, the power loss mainly refers to the conduction loss of the transistors since switching loss can be ignored due to soft switching; in the coils, the power loss is determined by their equivalent series resistances (ESRs), which can be measured by an LCR meter; in the capacitors, the power loss is also from their ESRs, which can be calculated by the dissipation factor and their impedance values at the frequency of interest. We take the fully aligned case as an example. Based on (4) and (6), the power loss in the fully aligned case is calculated as: inverter – 14 Watts, rectifier – 17 Watts, coils – 49 Watts, and capacitors – 48Watts. The total power loss is 138 Watts and the calculated efficiency is 84.30%, which is close to the experimental one, i.e., 86.19%. Furthermore, power loss in rotational misaligned cases is calculated and the results of the output power and DC-DC efficiency are compared with the experimental ones in Fig. 12. It is obvious that the calculated results match well with the experimental ones, so the circuit analysis is verified.

## V. Conclusion

A rotation-resilient wireless charging system with a two-part reversely wound receiver has been proposed in this paper. By reverse winding, the system performance on rotational misalignment is significantly improved, especially when large arc-shaped ferrite cores are employed. Finite element analysis has been conducted to verify the proposed idea and the circuit analysis has been performed. A prototype of the wireless charging system with the proposed coil structure has been built and

experimental results demonstrate that the output power on rotational misalignment is continuous with a maximum of 745 Watts and a minimum of 321 Watts. Furthermore, if customized arc-shape magnets are employed, the system output power can be even more constant during rotational misalignment.

## REFERENCE


[1] S. Li and C. C. Mi, "Wireless power transfer for electric vehicle applications," *IEEE J. Emerg. Sel. Topics Power Electron.*, vol. 3, no. 1, pp. 4–17, Mar. 2015.

[2] J. Huh, S. W. Lee, W. Y. Lee, G. H. Cho, and C. T. Rim, "Narrow-width inductive power transfer system for on-line electrical vehicles (OLEV)," *IEEE Trans. Power Electron.*, vol. 26, no. 12, pp. 3666–3679, Dec. 2011.

[3] Y. Zhang, K. Chen, F. He, Z. Zhao, T. Lu, and L. Yuan, "Closed-form oriented modeling and analysis of wireless power transfer system with constant-voltage source and load," *IEEE Trans. Power Electron.*, vol. 31, no. 5, pp. 3472–3481, Nov. 2015.

[4] S. Y. Hui, "Planar wireless charging technology for portable electronic products and Qi," *Proc. IEEE*, vol. 101, no. 6, pp. 1290–1301, Jun. 2013.

[5] D. Ahn and P. P. Mercier, "Wireless power transfer with concurrent 200 kHz and 6.78 MHz operation in a single transmitter device," *IEEE Trans. Power Electron.*, vol. 31, no. 7, pp. 5018–5029, Jul. 2016.

[6] S. Raju, R. Wu, M. Chan, and C. P. Yue, "Modeling of mutual coupling between planar Inductors in wireless power applications," *IEEE Trans. Power Electron.*, vol. 29, no. 1, pp. 481–490, Jan. 2014.

[7] C. Xiao, K. Wei, D. Cheng, and Y. Liu, "Wireless charging system considering eddy current in cardiac pacemaker shell: Theoretical modeling, experiments, and safety simulations," *IEEE Trans. Ind. Electron.*, vol. 64, no. 5, pp. 3978–3988, May 2017.

[8] P. P. Mercier and A. P. Chandrakasan, "Rapid wireless capacitor charging using a multi-tapped inductively-coupled secondary coil," *IEEE Trans. Circuits Syst. I, Reg. Papers*, vol. 60, no. 9, pp. 2263–2272, Sep. 2013.

[9] M. D. Feezor, F. Y. Sorrell, and P. R. Blankinship, "An interface system for autonomous undersea vehicles," *IEEE J. Ocean. Eng.*, vol. 26, no. 4, pp. 522–525, Oct. 2001.

[10] A. M. Bradley, M. D. Feezor, H. Singh, and F. Yates Sorrell, "Power systems for autonomous underwater vehicles," *IEEE J. Ocean. Eng.*, vol. 26, no. 4, pp. 526–538, Oct. 2001.

[11] T. Kojiya, F. Sato, H. Matsuki, and T. Sato, "Automatic power supply system to underwater vehicles utilizing non-contacting technology," in *Proc. Oceans MTTS/IEEE Techno-Ocean*, Nov. 2004, vol. 4, pp. 2341–2345.

[12] Z. Li, D. Li, L. Lin, and Y. Chen, "Design considerations for electromagnetic couplers in contactless power transmission systems for deep-sea applications," *J. Zhejiang Univ. Sci. C.*, vol. 11, no. 10, pp. 824–834, Sep. 2010.

[13] Z. Cheng, Y. Lei, K. Song, and C. Zhu, "Design and loss analysis of loosely coupled transformer for an underwater high-power inductive power transfer system," *IEEE Trans. Magn.*, vol. 51, no. 7, pp. 1–10, Jul. 2015.

[14] J. Shi, D. Li, and C. Yang, "Design and analysis of an underwater inductive coupling power transfer system for autonomous underwater vehicle docking applications," *J. Zhejiang Univ. Sci. C.*, vol. 15, no. 1, pp. 51–62, Jan. 2014.

[15] M. Lin, D. Li, and C. Yang, "Design of an ICPT system for battery charging applied to underwater docking systems," *Ocean Eng.*, vol. 145, no. 16, pp. 373–381, Nov. 2017.

[16] T. Kan, R. Mai, P. P. Mercier, and C. C. Mi, "Design and analysis of a three-phase wireless charging system for lightweight autonomous underwater vehicles," *IEEE Trans. Power Electron.*, vol. 33, no. 8, pp. 6622–6632, Aug. 2018.

[17] Z. Yan, K. Zhang, H. Wen, and B. Song, "Research on characteristics of contactless power transmission device for autonomous underwater vehicle," in *Proc. OCEANS*, 2016, pp. 1–5.

[18] S. Li, W. Li, J. Deng, T. Nguyen, and C. Mi, "A double-sided LCC compensation network and its tuning method for wireless power transfer," *IEEE Trans. Veh. Technol.*, vol. 64, no. 6, pp. 2261–2273, Jun. 2015.

[19] T. Kan, T. D. Nguyen, J. C. White, R. K. Malhan, and C. Mi, "A new integration method for an electric vehicle wireless charging system using LCC compensation Topology," *IEEE Trans. Power Electron.*, vol. 32, no. 2, pp. 1638–1650, Feb. 2017.

[20] R. L. Steigerwald, "A comparison of half-bridge resonant converter topologies," *IEEE Trans. Power Electron.*, vol. 3, no. 2, pp. 174–182, Apr. 1998.


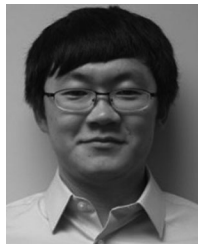

**Tianze Kan** (S'15) received the B.Eng. degree in electrical engineering and automation from Huazhong University of Science and Technology, Wuhan, China, in 2011 and the M.S. degree in electrical engineering from the University of Southern California, Los Angeles, CA, USA, in 2013. He is currently working toward the Ph.D. degree in electrical and computer engineering in the joint doctoral program between San Diego State University and the University of California San Diego, La Jolla, CA, USA.

His research interests include power electronics and inductive-based wireless power transfer, especially on coil design and compensation topologies.

**Yiming Zhang** (S'13–M'16) received the B.S. and Ph.D. degrees in electrical engineering from Tsinghua University, Beijing, China, in 2011 and 2016, respectively.

He is currently a Postdoctoral Researcher with San Diego State University, San Diego, CA 92182, USA. His research interests include wireless power transfer for electric vehicles and mobile phones, and resonant converters.

**Zhengchao Yan** (S'18) received the B.S. degree in mechanical design, manufacturing and automation from Northwestern Polytechnical University, Xi'an, China, in 2013, where he is currently working toward the Ph.D. degree. In 2017, he received the funding from China Scholarship Council, and became a joint Ph.D. student with the Department of Electrical and Computer Engineering, San Diego State University, San Diego, CA, USA.

His research interests focus on wireless power transfer including coil design and compensation topologies.

**Patrick P. Mercier** (S'04–M'12–SM'17) received the B.Sc. degree in electrical and computer engineering from the University of Alberta, Edmonton, AB, Canada, in 2006, and the S.M. and Ph.D. degrees in electrical engineering and computer science from the Massachusetts Institute of Technology, Cambridge, MA, USA, in 2008 and 2012, respectively.

He is currently an Assistant Professor in electrical and computer engineering with the University of California San Diego, where he is also the co-Director of the Center for Wearable Sensors. His research interests include the design of energy-efficient microsystems, focusing on the design of RF circuits, power converters, and sensor interfaces for miniaturized systems and biomedical applications.

**Chunting Chris Mi** (S'00–A'01–M'01–SM'03–F'12) received the B.S.E.E. and M.S.E.E. degrees in electrical engineering from Northwestern Polytechnical University, Xi'an, China, in 1985 and 1988, respectively and the Ph.D. degree in electrical engineering from the University of Toronto, Toronto, ON, Canada, in 2001.

He is a Professor and Chair of electrical and computer engineering and the Director of the Department of Energy funded Graduate Automotive Technology Education, Center for Electric Drive Transportation, San Diego State University (SDSU), San Diego, CA, USA. Prior to joining SDSU, he was with the University of Michigan, Dearborn from 2001 to 2015. His research interests include electric drives, power electronics, electric machines, renewable-energy systems, and electric and hybrid vehicles.